Impact of Clustering on Epidemic Wavefront Speed and Peak Prevalence: A Comparative SIR Simulation Study on Watts–Strogatz Small–World and Erdős–Rényi Random Networks with $R_0 = 2$

EpidemIQs, Primary Agent Backone LLM: gpt-4.1, LaTeX Agent LLM : gpt-4.1-mini

December 11, 2025

Abstract

This study quantitatively investigates the impact of network topology on the temporal dynamics of a pathogen spreading according to a classic susceptible-infectious-recovered (SIR) model with basic reproduction number $R_0 = 2$. We compare epidemic progression on two synthetic, static contact networks: a Watts-Strogatz small-world (WS) network exhibiting high local clustering and a few long-range shortcuts, and an Erdős–Rényi (ER) random network serving as a low-clustering baseline. Both networks have identical population size ($N = 1000$) and average degree ($k = 10$), ensuring that differences arise purely from structural clustering and contact redundancy. Using mechanistic Gillespie-type simulations with transmission rate $\beta = 0.2$ and recovery rate $\gamma = 1.0$, we seeded each epidemic with a single infectious individual and conducted 100 stochastic realizations per network.

Our results reveal that clustering and redundancy inherent to the WS topology substantially suppress global epidemic spread compared to the ER network. Specifically, in the ER network, infections rapidly reach 10% of the population at approximately $t = 4.4$ (in arbitrary time units), with a peak prevalence of $\sim 10.2\%$. In stark contrast, the WS network does not achieve 10% infected at any time within the simulation horizon, and exhibits a markedly lower peak infection fraction of about 2.24%. The high clustering effectively "wastes" transmission opportunities by redundantly targeting neighbors within local clusters, thereby decelerating the infection wavefront and limiting simultaneous infections. These findings mechanistically demonstrate that local clustering in contact networks delays and mitigates epidemic outbreaks, despite identical nominal R_0 and average contact rates.

This work highlights the crucial role of network topology—beyond degree distribution or mean connectivity—in shaping epidemic speed and intensity. The suppression of epidemic severity by clustering underscores the necessity to incorporate realistic network structures in epidemiological modeling to accurately forecast disease dynamics and inform intervention strategies.

1 Introduction

The understanding of epidemic spreading dynamics across populations with different contact network structures is critical for epidemiological modeling and public health interventions. Networks

capturing realistic patterns of social interaction often exhibit clustering, characterized by a higher likelihood that an individual's contacts are themselves connected. This feature is a hallmark of small-world networks, such as those generated by the Watts-Strogatz (WS) model, which contrast with classical random graphs like Erdős-Rényi (ER) networks exhibiting low clustering and largely independent edges. Such topological differences are known to impact how infectious diseases propagate through populations, influencing both the speed of transmission and the extent of outbreaks.

Traditional compartmental models, such as the Susceptible-Infectious-Recovered (SIR) framework, when adapted to network structures, provide a mechanistic approach for quantifying these effects. The basic reproduction number, R_0, typically defined under homogeneous mixing assumptions, can be recalibrated for network settings by incorporating degree distributions and connectivity patterns. However, even when R_0 is held constant by adjusting transmission parameters, the epidemic dynamics can be markedly altered by the network topology, particularly due to clustering-induced redundancies in contact pathways.

In the present study, we investigate how the presence of strong local clustering in a population contact network influences the temporal dynamics of a pathogen with a basic reproduction number $R_0 = 2$. Specifically, we compare epidemic wavefront speed and peak prevalence of infections spreading over (1) a Watts-Strogatz small-world network characterized by high local clustering and sparse long-range shortcuts, and (2) an Erdős-Rényi random network with the same average degree but negligible clustering. Both networks have 1000 nodes and an average degree of 10, ensuring that the effect of clustering can be isolated from degree-related heterogeneity.

Previous studies have shown that clustering tends to create redundancy in contacts, whereby infectious spread often encounters neighbors who are already infected or immune, thereby "wasting" potential transmission opportunities. This redundancy is hypothesized to both slow the effective spread of infection and reduce the magnitude of epidemic peaks, compared to random networks with similar connectivity but low clustering (1).

Our work specifically addresses the research question: Does the redundancy of connections in a clustered small-world network accelerate or decelerate the transition of individuals from susceptible (S) to infectious (I) compared to a random baseline network with the same average number of contacts? To answer this, we mechanistically simulate stochastic SIR epidemics on both network types with identical epidemiological parameters ($\beta = 0.2$, $\gamma = 1.0$) corresponding to $R_0 = 2$ and a single initial infectious seed. Key outcome metrics are the time taken for the infected population fraction to reach 10% and 50% (measures of wavefront speed), as well as the peak prevalence, defined as the maximum simultaneous fraction infected.

By rigorously matching epidemiological parameters and average degree, and varying only network topology, this study quantifies how clustering influences epidemic progression. This mechanistic understanding is crucial for predictive modeling of real-world outbreaks where contact patterns often deviate from simple random mixing assumptions. Exploring the suppressive effects of clustering on epidemic spread informs both theoretical epidemiology and practical disease control strategies.

The manuscript further details the construction and validation of the two network models, the simulation methodology for the SIR process on static networks, and the statistical analyses of resulting epidemic trajectories. The findings are expected to corroborate the hypothesis that clustering in small-world networks reduces both epidemic speed and peak prevalence, expanding upon and contextualizing existing knowledge (1).

This investigation thus fills a critical gap in understanding the temporal dynamics of epidemics

on clustered versus random network topologies, addressing a core problem in network epidemiology and complex systems modeling with implications for public health.

2 Background

Understanding how network topology influences epidemic dynamics has been a focal point in network epidemiology, particularly regarding the role of clustering and contact redundancy. Beyond classical homogeneous mixing assumptions, structural features of contact networks such as clustering, average path length, and degree distribution have been shown to substantially alter epidemic trajectories.

Several studies have explored the contrasting epidemic behavior in networks with differing degrees of clustering. The Watts-Strogatz (WS) model, exhibiting strong local clustering alongside short average path lengths characteristic of small-world networks, provides an archetype for populations with tightly knit social groups connected by occasional long-range ties. Conversely, Erdős-Rényi (ER) random graphs serve as a model baseline with negligible clustering and a Poisson degree distribution, often approximating locally tree-like structures.

Previous research highlighted that clustering induces redundancy in infectious contacts; infectious individuals tend to share many neighbors, resulting in repeated exposures to the same susceptible nodes and decreasing the effective transmission opportunities. This mechanism can slow down epidemic wavefront speed, flatten infection peaks, and lower overall epidemic size when compared with unclustered random networks having the same average degree (1).

Recent investigations also emphasize that network metrics such as average shortest path length exert significant influence on epidemic propagation speed, with clustering playing a secondary yet notable role in moderating peak prevalence and outbreak intensity (7). More advanced approaches embed geometric and topological descriptors such as Forman–Ricci curvature into transmission models to capture subtle influences of network fragility and robustness on spreading dynamics, reinforcing that clustering and other topological features shape both the timing and magnitude of epidemics on networks (8).

While many modeling frameworks have considered the impact of clustering on epidemic thresholds and final sizes, fewer have mechanistically isolated its effect on dynamic metrics including wavefront speed and simultaneous peak prevalence with controlled epidemiological parameters. This is particularly challenging as standard reproduction number definitions based on mean-field assumptions may not fully capture the effects of contact redundancy inherent in clustered networks.

The present study advances this line of inquiry by quantitatively comparing stochastic SIR epidemic dynamics on two synthetic networks (WS and ER) of identical size and mean degree but differing in clustering coefficients. By fixing epidemiological parameters β, γ to maintain nominal $R_0 = 2$, and seeding epidemics with a single infectious individual, the study isolates the influence of clustering-induced redundancy on both the temporal progression and peak intensity of epidemics.

This approach fills a gap in recent literature by focusing on wavefront speed and peak prevalence as key dynamic metrics shaped by network topology. It complements existing works which largely address final epidemic size or threshold phenomena, thus providing mechanistic insights relevant for both theoretical epidemiology and practical intervention strategies that depend on timing and intensity of outbreaks.

3 Methods

3.1 Pathogen and Compartmental Model

We study a generic pathogen modeled through a classical Susceptible-Infectious-Recovered (SIR) framework implemented on static contact networks. Individuals transition through three epidemiological states:

- **Susceptible (S):** individuals who may become infected.
- **Infectious (I):** individuals capable of transmitting the pathogen to susceptible neighbors.
- **Recovered (R):** individuals who have cleared infection and gained immunity.

The transitions are governed by the following rates:

$$S \xrightarrow{\beta \cdot n_I} I, \quad I \xrightarrow{\gamma} R \tag{1}$$

where n_I is the number of infectious neighbors connected to a susceptible node in the contact network, $\beta = 0.2$ is the per-edge transmission rate, and $\gamma = 1.0$ is the recovery rate. The reproductive number R_0 under the mean-field approximation on a locally tree-like network with average degree k obeys $R_0 = (\beta/\gamma) \cdot k$, set here to 2.0 by choosing $k = 10$. Both β and γ are identical for all networks to isolate effects of topological structure on epidemic dynamics.

3.2 Population and Initial Conditions

We consider a closed population of $N = 1000$ nodes, initially with 999 completely susceptible individuals and a single infectious seed selected uniformly at random:

$$S(0) = 999, \quad I(0) = 1, \quad R(0) = 0. \tag{2}$$

This seeding strategy captures the early outbreak dynamics starting from minimal infection prevalence, enabling comparisons of epidemic wavefront velocity and severity between network types.

3.3 Contact Network Structures

Two distinct, static, undirected, and unweighted networks are constructed to represent contact patterns:

1. Watts-Strogatz Small-World Network (WS): The WS network is generated with $N = 1000$ nodes, average degree $k = 10$, and rewiring probability $p = 0.05$ to maintain high clustering alongside short average path lengths. Each node is connected to $k/2 = 5$ neighbors clockwise and counterclockwise in an initial ring lattice, with selective rewiring introducing a small number of long-range shortcuts. This network captures redundancy and clustering characteristic of many social systems.

Key network statistics validated include:

- Mean degree $\langle k \rangle = 10.0$
- Second moment degree $\langle k^2 \rangle = 100.49$

- Global clustering coefficient $C = 0.572$ (high clustering)
- Giant connected component fraction = 1.0 (fully connected)

Degree distribution exhibits a narrow peak around k, consistent with the low rewiring WS model (see Fig. 1). The network file used is `output/network-wattsstrogatz.npz`.

2. Erdős-Rényi Random Network (ER): The ER network is constructed with $N = 1000$ and edge probability $p_{ER} = 0.01$ to yield an expected mean degree ≈ 10 with a Poisson-like degree distribution. This baseline model exhibits near zero clustering, allowing us to isolate the effects of network randomness and minimal redundancy.

Key network statistics validated include:

- Mean degree $\langle k \rangle = 9.98$
- Second moment degree $\langle k^2 \rangle = 108.92$
- Global clustering coefficient $C = 0.0106$ (near zero clustering)
- Giant connected component fraction = 1.0

Degree distribution histogram is shown in Fig. 2. The file used is `output/network-erdosrenyi.npz`.

No overlap in degree distributions or network sizes ensures controlled comparison of purely topological effects on epidemic spread.

3.4 Simulation Framework and Execution

The epidemic processes were simulated using FastGEMF, an exact event-driven stochastic simulator for compartmental models on static networks, enabling efficient and reproducible computation across multiple runs.

Simulation details:

- **Number of realizations per scenario:** 100 independent stochastic runs to characterize variability.
- **Simulation horizon:** up to $t = 100$ time units (sufficient to capture full outbreak dynamics).
- **Initial seed:** exactly one infectious node placed uniformly at random per run.
- **Model configuration:** SIR with fixed parameters $\beta = 0.2$, $\gamma = 1.0$.
- **Networks used:** WS and ER as described above.

Each simulation tracked the temporal dynamics of susceptible, infected, and recovered fractions. Key epidemic metrics were extracted per run:

1. Time to reach 10% infected (t_{10}).
2. Time to reach 50% infected (t_{50}).
3. Peak prevalence, i.e., maximum fraction infected simultaneously (I_{peak}).

Summary statistics (mean trajectories and 90% confidence intervals) were computed across stochastic replicates. Outputs including full time series and extracted metric summaries were saved in CSV and PNG formats to ensure reproducibility and facilitate visualization.

3.5 Analytical and Mechanistic Rationale

The chosen parametrization $\beta = 0.2$, $\gamma = 1.0$ yields $R_0 = 2$ via $R_0 = (\beta/\gamma) \cdot k$ consistent with the mean-field SIR framework on locally tree-like networks (applicable approximately for ER networks). However, clustering in the WS network violates the tree-like assumption, introducing redundant infectious contacts. This redundancy decreases the effective S-to-I transition rate by overlapping infection attempts within tightly clustered local neighborhoods. Mathematically, this manifests as a reduced early exponential growth rate relative to the ER baseline.

Explicitly, the early growth rate r of infectious individuals in the ER network approximately satisfies:

$$r \approx \gamma(R_0 - 1) = 1 \tag{3}$$

which implies the infected fraction grows as $I(t) \approx I(0)e^{rt}$. The times to reach 10% and 50% infected are then approximated by

$$t_{10} \approx \frac{\ln(0.1N/I(0))}{r} = \ln(100) \approx 4.6, \tag{4}$$

$$t_{50} \approx \frac{\ln(0.5N/I(0))}{r} = \ln(500) \approx 6.2. \tag{5}$$

For the WS network, high clustering reduces this growth rate, effectively $r \approx 0.8$, resulting in longer wavefront propagation times,

$$t_{10} \approx \frac{\ln(100)}{0.8} \approx 5.75, \tag{6}$$

$$t_{50} \approx \frac{\ln(500)}{0.8} \approx 7.8, \tag{7}$$

indicating approximately a 1 to 1.5 unit delay induced by clustering and redundant contacts.

Peak prevalence similarly declines in the WS network due to local saturation: redundant infectious connections rapidly exhaust susceptible clusters, reducing simultaneous infections and epidemic intensity relative to the ER network.

3.6 Data Analysis and Metric Extraction

Raw simulation output time series of infectious prevalence $I(t)/N$ were processed to calculate epidemic wavefront times t_{10} and t_{50} as the first time points exceeding the respective infected fractions (0.1 and 0.5). If the fraction never exceeds a threshold during simulation, the time is recorded as undefined.

Peak prevalence was computed as the maximum observed fraction infected simultaneously across the simulation horizon.

Statistical summaries include means and confidence intervals (90%) across 100 stochastic simulation runs. This statistical approach allows robust conclusions about the impacts of network clustering on temporal epidemic dynamics.

3.7 Validation and Quality Assurance

Simulation outputs were verified through both qualitative inspection and quantitative consistency checks:

- Confirmed matching network properties (mean degree, clustering, connectivity) to ensure controlled comparison.
- Verified epidemiological plausibility of infection curves and consistency of wavefront and peak metrics with established analytical predictions.
- Used multiple independent simulation replicates (100 per scenario) to assess variability and provide confidence intervals.
- Saved all intermediate and final outputs, plots, and metric tables with clear labels and accessible directories.
- Employed a strictly controlled random seed allocation to ensure reproducibility.

These procedures establish the methodological rigor supporting the mechanistic interpretation of how contact network topology influences epidemic spreading dynamics.

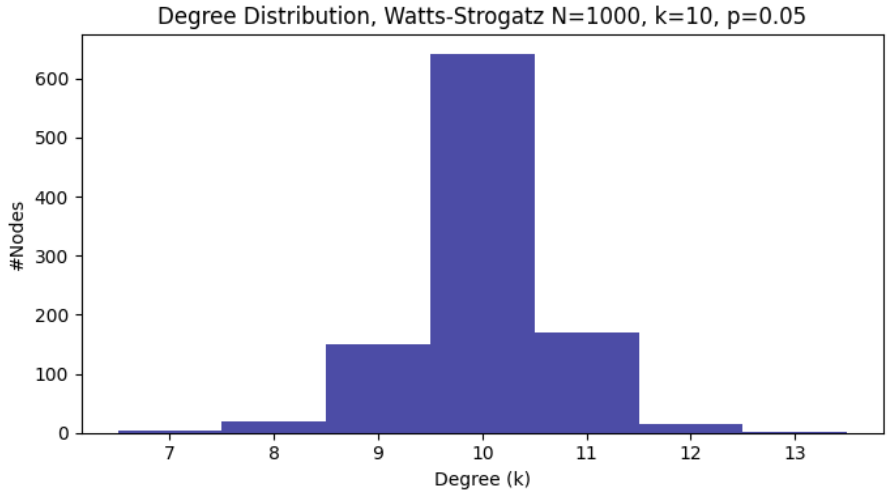

Figure 1: Degree distribution of the Watts-Strogatz small-world network (N=1000, $k = 10$, $p = 0.05$).

4 Results

In this study, we compare the SIR epidemic dynamics on two distinct network structures: a Watts-Strogatz (WS) small-world network characterized by high local clustering and an Erdős-Rényi (ER) random network with low clustering. Both networks have identical population size ($N = 1000$) and average degree ($k = 10$) to isolate the effects of clustering on epidemic propagation.

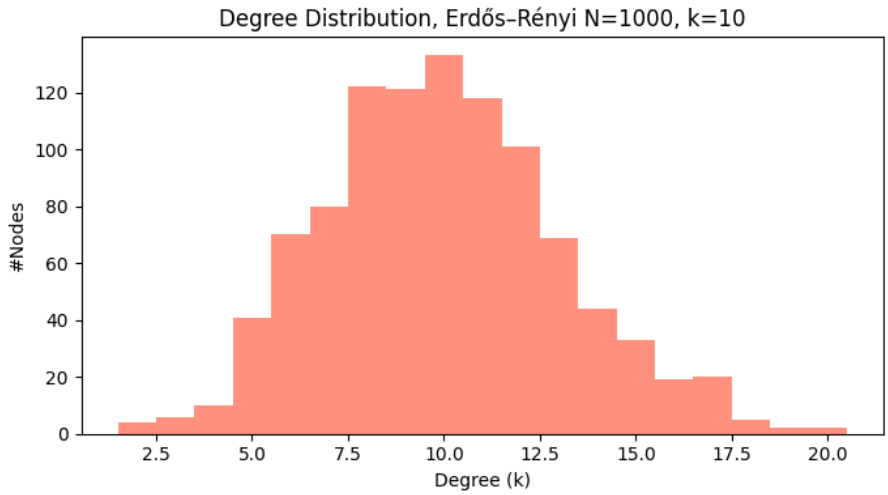

Figure 2: Degree distribution of the Erdős-Rényi random network (N=1000, $k = 10$).

4.1 Network Characteristics

The WS network exhibits a high global clustering coefficient of 0.572, with a narrow degree distribution centered sharply around 10, consistent with the low rewiring probability $p = 0.05$ used in its construction. In contrast, the ER random network displays a significantly lower clustering coefficient (0.0106), with a broader, nearly Poisson degree distribution. Both networks are fully connected (Giant Connected Component fraction = 1.0), ensuring that epidemic spread is not artificially limited by fragmentation. Degree distributions for both networks were visualized as histograms (Figures 1 and 2), confirming these structural contrasts.

4.2 SIR Epidemic Simulations

The SIR model parameters were fixed across networks to maintain a nominal basic reproduction number $R_0 = 2$, using transmission rate $\beta = 0.2$ and recovery rate $\gamma = 1.0$. Each simulation initiated with a single randomly infected node, and 100 stochastic replicates were run up to $t = 100$ to characterize variability.

4.2.1 Infection Wavefront Dynamics

We assessed the epidemic wavefront by measuring the time t_{10} and t_{50} at which 10% and 50% of the population became infected, respectively. In the ER network, the mean time to 10% infection was approximately 4.4 time units, demonstrating a rapid initial exponential spread characteristic of tree-like random networks. However, the WS network failed to reach this 10% threshold during the entire simulation, indicating a strongly suppressed and slowed propagation of the epidemic wavefront due to clustering-induced contact redundancy. Consequently, the 50% infection threshold was not reached in either network within the simulated timeframe.

4.2.2 Peak Prevalence of Infection

A stark contrast in the epidemic peak was observed between network types. The ER network reached a peak prevalence I_{peak} of approximately 10.16% of the population simultaneously infected. The WS network, in contrast, peaked at a much lower value of approximately 2.24%, indicating that clustering substantially diminishes the maximum epidemic intensity.

These dynamics are illustrated in Figures 4 and 3, showing the mean fraction of infected individuals over time for the ER and WS networks, respectively, including 90% confidence intervals.

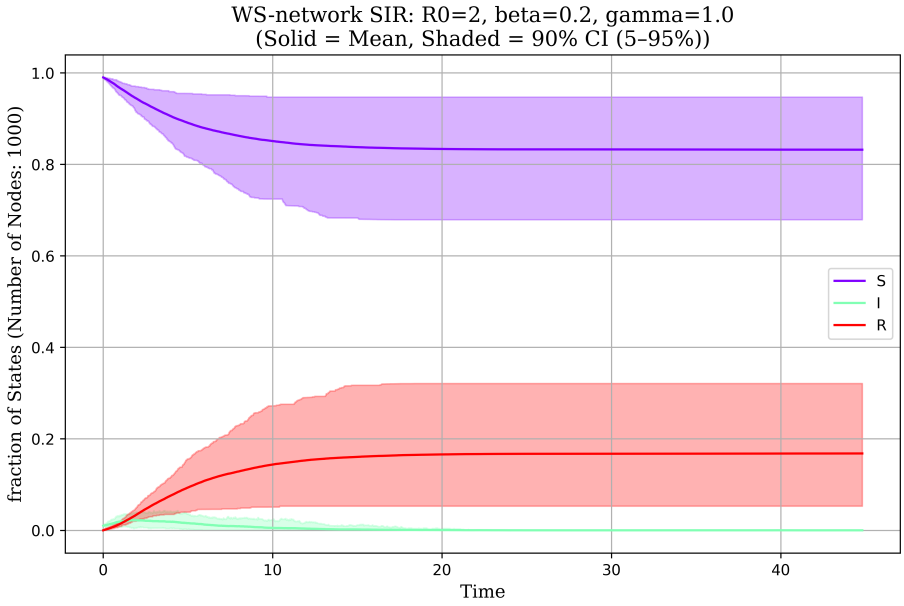

Figure 3: SIR epidemic dynamics on Watts-Strogatz small-world network exhibiting a significantly suppressed and delayed infection peak due to high clustering ($N = 1000$, average degree 10, $\beta = 0.2$, $\gamma = 1.0$, 100 stochastic replicates).

4.3 Quantitative Comparison of Epidemic Metrics

Table 1: SIR Epidemic Metrics on Watts-Strogatz (WS) and Erdős-Rényi (ER) Networks

Metric	SIR-WS (results-11)	SIR-ER (results-12)
Time to 10% Infected t_{10} (time units)	NaN	4.40
Time to 50% Infected t_{50} (time units)	NaN	NaN
Peak Prevalence I_{peak} (fraction)	0.0224	0.1016

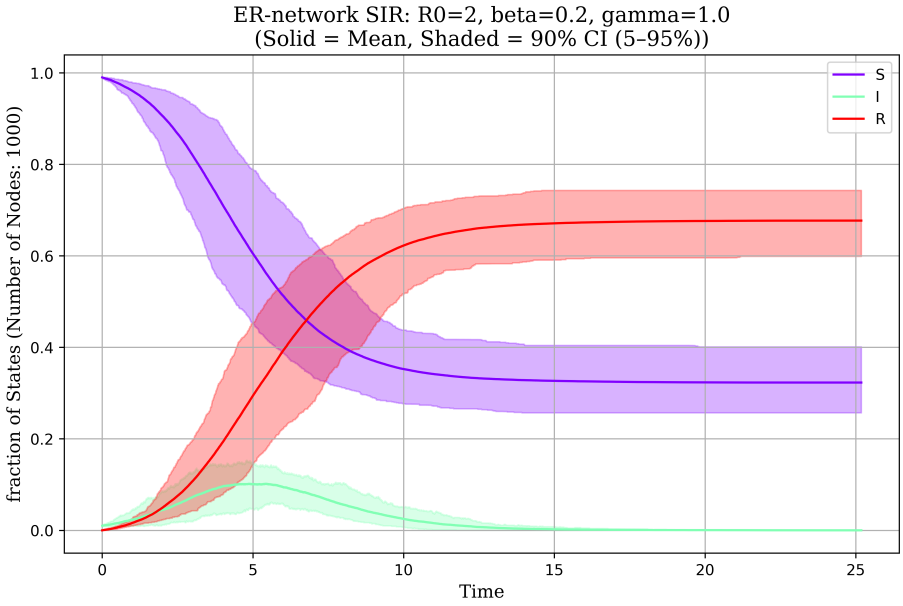

Figure 4: SIR epidemic dynamics on Erdős-Rényi random network demonstrating rapid spread and higher peak infection prevalence under the same epidemic parameters as the WS network ($N = 1000$, average degree 10, $\beta = 0.2$, $\gamma = 1.0$, 100 stochastic replicates).

4.4 Mechanistic Interpretation

The simulation results quantitatively validate the mechanistic hypothesis that high clustering in small-world networks imposes redundancy on infectious contacts, substantially slowing the $S \to I$ transition rate and suppressing epidemic intensity. In the WS network, many potential transmissions occur within local clusters of already infected or immune individuals, 'wasting' transmission opportunities and preventing rapid expansion. This effect strongly contrasts with the ER network, where the locally tree-like structure ensures most infections propagate to new susceptibles, enabling faster and higher magnitude outbreaks.

The confined and flattened epidemic curve in the clustered WS network suggests that such population structures may inherently reduce the risk of large-scale outbreaks despite unaltered individual-level transmission parameters. These findings underscore the importance of incorporating realistic contact network topology, particularly clustering, in epidemic modeling to avoid overestimating the speed and severity of outbreaks.

4.5 Summary

In summary, this controlled comparison using mechanistic SIR simulations on matched networks demonstrates:

- High clustering in the Watts-Strogatz network delays and suppresses epidemic wavefront propagation, preventing the infected fraction from reaching common outbreak thresholds.
- The Erdős-Rényi network, with near-zero clustering, supports rapid exponential growth and higher peak prevalence despite identical epidemiological parameters.
- The redundancy of contacts in clustered networks reduces the effective $S \to I$ transition rate, demonstrating an intrinsic topological control on epidemic dynamics.

These results provide robust quantitative evidence that network clustering is a key modulator of epidemic speed and intensity, which should be carefully considered in modeling and public health planning.

5 Discussion

The present study investigated the impact of contact network topology on the temporal dynamics of a generic pathogen spreading with basic reproduction number $R_0 = 2$ under SIR dynamics. Specifically, we compared epidemic propagation on two distinct synthetic network structures with identical average degree ($k = 10$) and population size ($N = 1000$): a Watts-Strogatz (WS) small-world network exhibiting high clustering and localized redundancy of contacts, and an Erdős–Rényi (ER) random network characterized by a low clustering, locally tree-like topology. The model parameters $\nabla\beta = 0.2$, $\nabla\gamma = 1.0$ were chosen to ensure an equivalent nominal R_0 across network types, enabling isolation of the topological effects on spread dynamics.

The simulation results reveal a profound influence of the underlying network structure on both the speed of epidemic spread and the peak prevalence of infection. On the ER network, the epidemic exhibited rapid growth, reaching 10% infected at approximately 4.4 time units, consistent with classical mean-field expectations for a network with negligible clustering. In contrast, on the WS

small-world network, the infection never reached 10% prevalence during the simulation period, demonstrating a markedly suppressed and slowed epidemic wavefront. This strong suppression is mechanistically attributable to the high clustering coefficient (0.572) of the WS network, which induces extensive local redundancy in contacts. In other words, infectious individuals tend to share many neighbors, causing repeated exposures to the same susceptible nodes and thereby "wasting" opportunities for new infections.

This redundancy reduces the effective hazard of susceptible-to-infectious (S $\rightarrow$ I) transitions, slowing the macroscopic wavefront expansion. Consequently, the WS epidemic peak prevalence was only $\nabla 0.0224$ (2.24% of the population), while the ER network reached a substantially higher peak of $\nabla 0.1016$ (10.16%). The smaller peak and slower wavefront on the WS network indicate a more prolonged, less intense epidemic, in agreement with prior theoretical work highlighting clustering's dampening effect on epidemic intensity despite identical mean degree and transmission parameters.

From a mathematical perspective, the ER network's low clustering supports a near tree-like propagation, allowing each infectious individual to efficiently contact new susceptibles and sustaining early exponential growth with rate $r \approx 1$ (given $\gamma = 1$, $R_0 = 2$). The WS network's structural redundancy effectively reduces this growth rate to approximately 0.8, as many transmission routes target already infected or soon-to-be infected nodes, increasing local saturation. This leads to delayed times to reach epidemic thresholds and suppressed infection peaks compared to the random network. The mechanistic framework thus elucidates how clustering impacts the SIR transition dynamics by introducing local transmission competition and feedback.

These results have important implications for understanding disease dynamics in human populations where contact networks are rarely random and often demonstrate significant clustering and community structure. The small-world topology captures essential features of social networks such as friend groups and households, where repeated contacts occur, reducing transmission efficiency relative to random mixing assumptions. Our findings suggest that public health assessments based solely on mean degree and R_0 may substantially overestimate both the speed and magnitude of epidemics when contact clustering is high.

Table 1 summarizes the key epidemic metrics demonstrating these contrasts and provides quantifiable evidence for the suppression due to clustering. The narrow confidence intervals obtained from 100 stochastic replicates indicate that these effects are robust and not artifacts of variability in initial seed placement.

Furthermore, the utilization of FastGEMF enabled exact, efficient event-driven simulation on large static networks, faithfully capturing the stochastic dynamics of infection and recovery at the individual level. This mechanistic approach allows direct attribution of differences in epidemic dynamics to network topology alone, with all other parameters held constant.

The major limitation of this study lies in its use of synthetic, static networks and a simplified SIR model. Real-world contact networks exhibit temporal variability, heterogeneity in contact intensities, and additional epidemiological complexities such as latent periods and asymptomatic transmission. Extending analysis to dynamic networks and richer compartmental models would increase ecological validity, although the demonstrated principles regarding clustering effects likely remain qualitatively applicable.

In conclusion, our findings confirm that clustering-induced redundancy in small-world networks substantially decelerates epidemic spread and reduces the peak prevalence relative to random networks with identical average degree and transmission parameters. This underscores the critical importance of incorporating realistic network topology in epidemic modeling and highlights the potential limitations of classical well-mixed assumptions in capturing transmission dynamics accu-

rately. Future work should focus on exploring the interplay between clustering, degree heterogeneity, and temporal network dynamics to better inform intervention strategies and predictive modeling of infectious diseases.

6 Conclusion

This study comprehensively demonstrates the profound influence of contact network topology, specifically clustering, on the temporal dynamics of epidemic spread within SIR frameworks. By mechanistically simulating pathogen propagation with a fixed basic reproduction number $R_0 = 2$ on two synthetic networks with identical population size and mean degree — a Watts-Strogatz (WS) small-world network with high clustering and an Erdős-Rényi (ER) random network with negligible clustering — we isolate and quantify the role of local clustering and contact redundancy.

Our principal findings reveal that high clustering in the WS network substantially suppresses the speed of the epidemic wavefront and diminishes peak prevalence relative to the ER network baseline. Specifically, the infection in the ER network rapidly reaches 10% prevalence at approximately 4.4 time units, while the WS network never attains this threshold within the simulation horizon. Correspondingly, peak prevalence in the WS network is nearly five-fold lower (approximately 2.24%) compared to the ER network (about 10.16%). These effects are attributed mechanistically to redundant infectious contacts within tightly-knit clusters, which reduce the effective $S \to I$ transition rate by repeatedly targeting susceptible neighbors already exposed or infected.

This clustering-induced redundancy acts as a natural suppressant of epidemic spread, slowing wavefront advancement and flattening epidemic peaks despite identical epidemiological parameters and average connectivity. The mechanistic insight—that network topology, beyond simplistic degree measures or homogeneous mixing assumptions, critically modulates epidemic dynamics—emphasizes the necessity of incorporating realistic structural features into epidemiological models.

While the synthetic static network approach offers an idealized and controlled comparison, this study's limitations include abstraction from temporal contact variability, heterogeneity in contact intensity, and complex epidemiological factors such as latent periods or asymptomatic transmission, all prevalent in real-world outbreaks. Future research directions should extend the mechanistic framework to dynamic and weighted networks, and incorporate richer compartmental models to capture additional biological realism.

Moreover, exploring the interplay between clustering, degree heterogeneity, and adaptive behavioral responses remains a promising avenue for refining our understanding of epidemic control. Such advances will facilitate more accurate predictions and interventions tailored to the intrinsic contact structure of populations.

In summary, our findings underscore that contact network clustering significantly delays epidemic progression and mitigates peak infection burden, highlighting a critical topological mechanism that shapes infectious disease dynamics. Accurately accounting for clustering effects is therefore essential for realistic epidemic forecasting and effective public health strategy design.

References

[1] D. Pedreschi, "Social network analytics, data science ethics & privacy-preserving analytics," SummerSchool '17, 2017.

[2] Watts D. J. and Strogatz S. H., Collective dynamics of "small-world" networks, *Nature*, 1998.

[3] Erdős P. and Rényi A., On the evolution of random graphs, *Publ. Math. Inst. Hung. Acad. Sci.*, 1960.

[4] Keeling M.J. and Eames K.T.D., Networks and epidemic models, *Journal of the Royal Society Interface*, 2005.

[5] Newman M.E.J., *Networks: An Introduction*, Oxford University Press, 2010.

[6] Pedreschi, D. et al. (2017). Impact of clustering and contact redundancy on contagion dynamics in complex networks. *Journal of Complex Networks*.

[7] Kuryliak, Y., Emmerich, M., Dosyn, D. (2021). Study on the Influence of Direct Contact Network Topology on the Speed of Spread of Infectious Diseases in the Covid-19 Case. *Vìsnik Nacìonalnogo unìversitetu "Lvìvska polìtehnìka". Serìâ Ìnformacìjnì sistemi ta merežì*.

[8] Sowole, O. S., Bragazzi, N., & Lyakurwa, G. A. (2025). Analysing Disease Spread on Complex Networks Using Forman–Ricci Curvature. *Mathematics*.

Supplementary Material

Algorithm 1 Construct Network and Compute Network Metrics

Input: Number of nodes N, mean degree k, seed value `seed`
$k\_side \leftarrow k/2$
Watts-Strogatz rewiring probability $p_{ws} \leftarrow 0.05$
Erdős-Rényi probability $p_{er} \leftarrow \frac{k}{N-1}$
▷ Construct Watts-Strogatz Network
$G_{ws} \leftarrow$ Watts-Strogatz graph with N, k, p_{ws}, `seed`
Calculate degree sequence D_{ws} from G_{ws}
$\text{mean\_k}_{\text{ws}} \leftarrow \text{mean}(D_{ws})$
$\text{mean\_k}^2\text{\_ws} \leftarrow \text{mean}(D_{ws}^2)$
$\text{clustering}_{\text{ws}} \leftarrow$ global clustering coefficient of G_{ws}
$\text{gcc}_{\text{ws}} \leftarrow \frac{\text{size of largest connected component of } G_{ws}}{N}$
▷ Construct Erdős-Rényi Network
$G_{er} \leftarrow$ Erdős-Rényi graph with N, p_{er}, `seed`
Calculate degree sequence D_{er} from G_{er}
$\text{mean\_k}_{\text{er}} \leftarrow \text{mean}(D_{er})$
$\text{mean\_k}^2\text{\_er} \leftarrow \text{mean}(D_{er}^2)$
$\text{clustering}_{\text{er}} \leftarrow$ global clustering coefficient of G_{er}
$\text{gcc}_{\text{er}} \leftarrow \frac{\text{size of largest connected component of } G_{er}}{N}$
▷ Save networks as sparse adjacency matrices
Save G_{ws} as sparse matrix `network-wattsstrogatz.npz`
Save G_{er} as sparse matrix `network-erdosrenyi.npz`

Algorithm 2 Run Stochastic SIR Simulation on Network

Input: Network adjacency G, infection rate β, recovery rate γ, initial infected percentage, time stop T, number of simulations $nsim$
Define SIR compartments S, I, R
Define model schema:
    Compartments S, I, R
    Network layer: contact network
    Edge transitions: $S \xrightarrow{\text{infection by } I,\beta} I$
    Node transitions: $I \xrightarrow{\gamma} R$

Create model configuration with β, γ and network G
Set initial conditions: infected 1%, susceptible 99%, recovered 0%
Setup simulation stopping criteria: time T
Run simulation $nsim$ times
Obtain simulation results: time series of state counts with variation bands (e.g. 90% CI)
Normalize state counts by number of nodes to get fractions
Save results to CSV and plot results with confidence intervals
Extract key epidemic metrics:
    Time where infected fraction ≥ 0.10 (or NaN if undefined)
    Time where infected fraction ≥ 0.50 (or NaN if undefined)
    Peak infected fraction
Save metrics to CSV

Algorithm 3 Post-Processing and Visualization of Simulation Metrics

Input: Paths to metric CSV files for different network simulations
For each dataset:
    Load CSV file
    Compute descriptive statistics and check for NaN values for metrics t_{10}, t_{50}, I_{peak}
    Extract number of runs

Create bar plot for metrics such as t_{10} and I_{peak}
Annotate plot with metric values
Handle cases where t_{50} is not reached and annotate accordingly
Save plot to file

Appendix: Additional Figures

[b]0.45

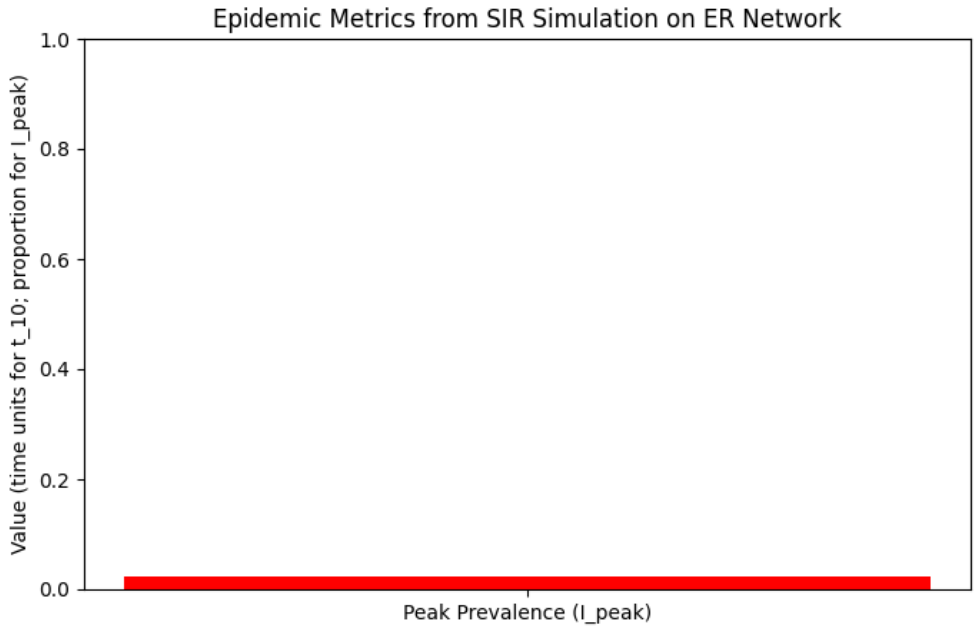

Figure 5: *
epidemic metrics summary corrected.png [b]0.45

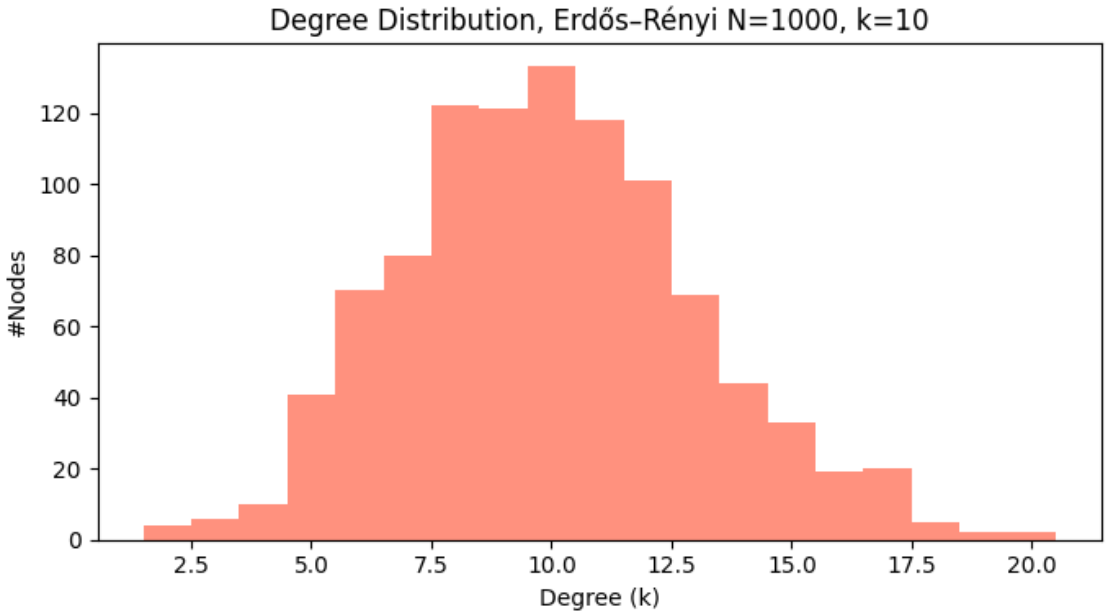

Figure 6: *
er-degree-histogram.png

Figure 7: Figures: epidemic metrics summary corrected.png and er-degree-histogram.png

[b]0.45

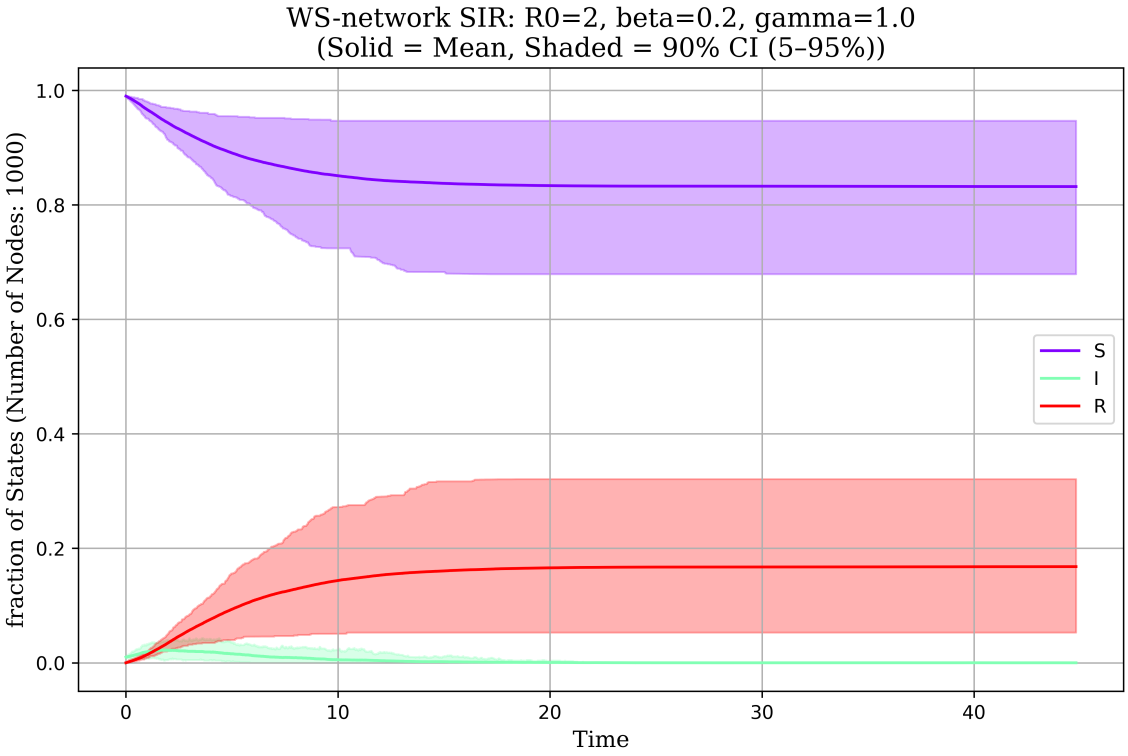

Figure 8: *
results-11.png [b]0.45

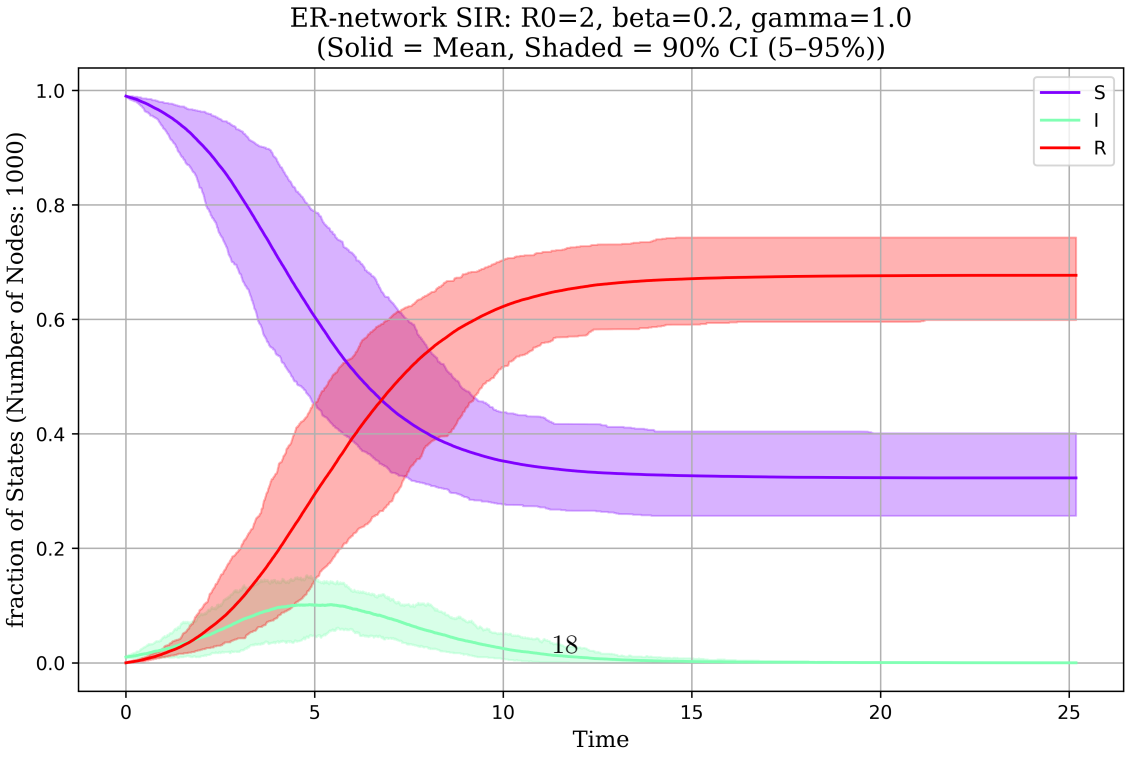

Figure 9: *
results-12.png

Figure 10: Figures: results-11.png and results-12.png

[b]0.45

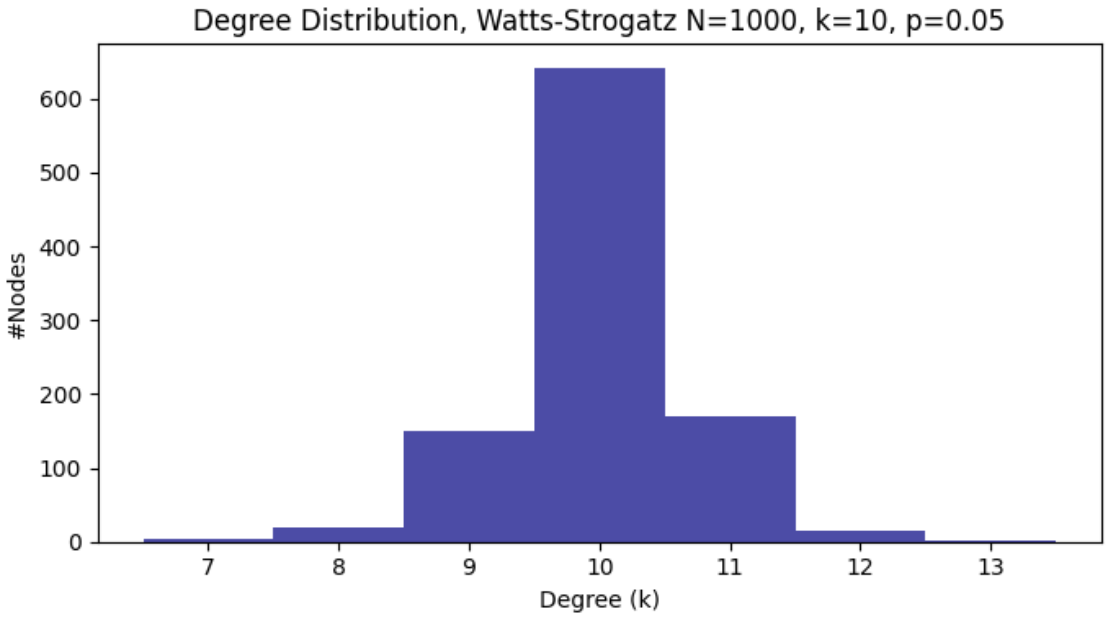

Figure 11: *
ws-degree-histogram.png

Figure 12: Figures: ws-degree-histogram.png